PROCEEDINGS OF SCIENCE

Impact of the Galactic magnetic field modeling on studies of the UHECRs arrival direction

Luca Deval,[a,*] **Ralph Engel,**[a] **Thomas Fitoussi,**[a] **Esteban Roulet**[b] **and Michael Unger**[a]

[a] *Karlsruhe Institute of Technology, Karlsruhe, Germany*

[b] *Centro Atómico Bariloche, Bariloche, Argentina*

E-mail: luca.deval@gmail.com

Ultra-high energy cosmic rays (UHECRs) are charged particles of extreme energy that experience deflections in Galactic and extragalactic magnetic fields as they propagate to Earth. These deflections limit the ability to trace their arrival directions back to their sources.

In this work, we investigate the impact of Galactic magnetic deflections on cross-correlation analyses with source catalogs by modeling different configurations of the turbulent and coherent fields. We show that even when magnetic deflections are applied to simulated data, the best-fit parameters found by the Pierre Auger Collaboration for the correlation with starburst galaxies can be recovered with high probability. However, a search for local overdensities in the simulations predicts secondary structures that are absent in the data. By comparing data and simulations, we demonstrate how these analyses can constrain the strength of the extragalactic magnetic field.

7th International Symposium on Ultra High Energy Cosmic Rays (UHECR2024)
17-21 November 2024
Malargüe, Mendoza, Argentina

*Speaker

ISSN 1824-8039. Published by SISSA Medialab.

PoS(UHECR2024)080

1. Introduction

Ultra-high-energy cosmic rays (UHECRs) are charged particles with energies above 10^{19} eV, whose sources remain unknown. Recent studies have explored correlations between source populations and the arrival directions of these particles. The latest analysis by the Pierre Auger Collaboration found that cross-correlation with the starburst galaxy (SBG) catalog from [1] provides the best agreement with observed data, with a significance of 4σ [2]. However, this study did not account for deflections caused by Galactic and extragalactic magnetic fields (GMF and EGMF, respectively).

In this work, we generate simulated datasets that account for magnetic field deflections, which play a crucial role in UHECR propagation and arrival directions. We then perform a maximum likelihood analysis on these simulations to assess whether the correlation with SBGs persists under the influence of GMF deflections. In addition to studying the correlation with the source catalog, we analyze the properties of localized excesses, aiming to compare the results with data and constrain the strength of these magnetic fields.

2. Maximum likelihood analysis

To incorporate the effects of magnetic fields in our analysis, we construct simulated datasets for each starburst galaxy (SBG) in the catalog. These simulations assume a mixed composition spectrum injected at the source, consistent with the EPOS-LHC best-fit parameters presented in [3], and a cosmic-ray flux proportional to the radio flux of SBGs at 1.4 GHz. The energy losses of charged particles as they propagate through extragalactic photon fields are accounted for using one-dimensional simulations with `CRPropa3` [4]. The deflections induced by the Galactic magnetic field (GMF) are modeled using the Jansson & Farrar (`JF12`) model [5] and the UF23 ensemble [6]. The turbulent component is modeled using either the initial `JF12` model parameters [7] or the updated values from Ref.[8]. These deflections are applied to the simulated cosmic rays using a lensing technique [9], allowing us to realistically assess their impact on arrival directions. By incorporating these effects, we aim to evaluate whether the observed correlation between UHECR arrival directions and the SBG catalog remains significant after accounting for magnetic field distortions.

To investigate how variations in the background affect the likelihood analysis, we generate multiple realizations with different signal contributions. Specifically, we define the number of signal events in each dataset as

$$N_{\rm sig} = f_{\rm ani} \times N_{\rm data}, \tag{1}$$

where $f_{\rm ani}$ represents the anisotropic fraction, and $N_{\rm data}$ is the total number of observed cosmic-ray events above the energy threshold of 38 EeV ($N_{\rm data} = 1621$). We construct 1000 random realizations of Auger data by combining these signal events with an isotropic background. For each realization, we apply a maximum likelihood analysis that compares a model sky map, n^{H_1}, to a null hypothesis represented by an isotropic sky, n^{H_0}. In the model sky map, a von Mises-Fisher distribution is applied around each source with a search radius θ and scaled by the anisotropic fraction α. The test

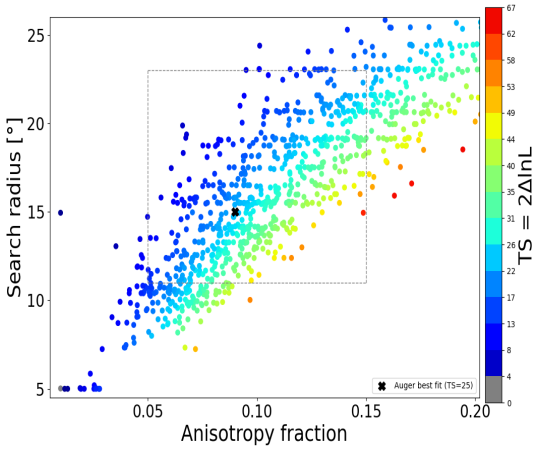

(a) Fitted anisotropy fraction and search radius for 1000 realizations with a generated signal fraction of 15%.

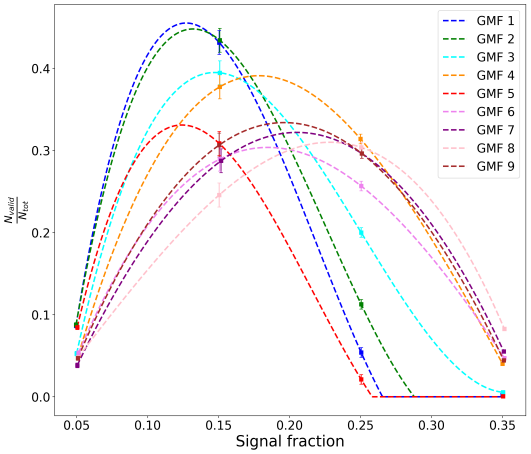

(b) Fraction of compatible datasets as a function of the signal source contribution for different realizations of the turbulent magnetic field.

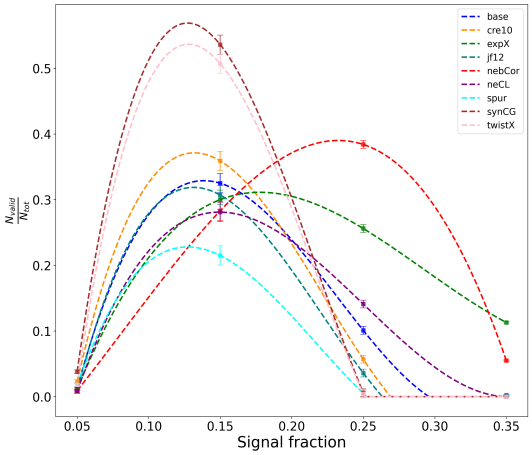

(c) Fraction of compatible datasets as a function of the signal source contribution for different models of the coherent magnetic field in the UF23 ensemble and `JF12`.

Figure 1: Results of the maximum likelihood analysis applied to simulated datasets.

statistic (TS) is computed as

$$\mathrm{TS} = 2 \sum_i k_i \times \ln \frac{n^{H_1}}{n^{H_0}}, \tag{2}$$

where k_i is the number of events in direction i, using a `HEALPix` grid with n_{side}=64, corresponding to a pixel size of approximately 1°. To account for Galactic variance, we consider nine different realizations of the turbulent magnetic field of Ref.[7] and study their effect on the computed TS values. The results of our analysis are presented in Fig. 1.

Fig. 1a displays the best-fit parameters obtained for each realization, along with the corresponding TS values. The dashed gray lines define the region of interest, where simulated datasets are considered compatible if their best-fit parameters fall within the uncertainties reported in Ref.[2].

The best-fit parameters obtained in the Auger analysis are marked with a black cross. To further refine the selection, we impose an additional constraint on the TS value, requiring it to be within the range $13 \leq \mathrm{TS} \leq 34$, ensuring that only statistically consistent scenarios are considered.

Fig. 1b illustrates the influence of different realizations of the turbulent GMF on the fraction of compatible datasets assuming `JF12` as the coherent field as well as the original `JF12` turbulent field strength. While the overall trend remains consistent across realizations, the percentage of valid simulated scenarios varies between approximately 30% and 40%, highlighting the significant role of Galactic variance in determining the likelihood of a successful correlation. Similarly, variations in the coherent field component within the UF23 ensemble show a comparable overall behavior across different models, while the fraction of valid scenarios ranges from approximately 20% to 50%, as presented in Fig. 1c.

An important aspect of our findings is the relationship between the true signal contribution and the fitted anisotropic fraction. We observe that the highest number of compatible realizations occurs for a true anisotropic fraction in the range of $15\% - 25\%$, whereas the best-fit value reported in Ref.[2] is 9%. This discrepancy arises from the composition of the injected cosmic rays: the simulations assume a mixture of 60% nitrogen and 40% silicon. Due to their lower rigidity, silicon nuclei experience stronger deflections and become effectively isotropized in the turbulent field, thereby contributing as an additional background. As a result, a larger true source fraction is required to reproduce the observed anisotropic signal. Overall, the results obtained show that including GMF deflections in UHECR arrival direction modeling, together with the SBG catalog as a source population, leads to simulated datasets that are statistically compatible with Auger data. This finding is consistent with the results reported in Ref.[10], showing that a correlation between UHECRs and starburst galaxies can still be found after including the influence of magnetic deflections.

3. Intermediate-angular-scale anisotropies in the UHECR sky

Another important aspect of our analysis concerns the strength and characteristics of localized excesses at intermediate-angular scale. To quantify the excess in different regions of the sky, the local significance is computed by comparing the number of observed events within a given top-hat search radius to the expected number of isotropic events in the same angular window, following binomial statistics. To systematically identify significant overdensities, we perform a sequential angular scan. The first scan determines the position and amplitude of the most significant hotspot (σ_1), after which the surrounding region is excluded. A second scan is then performed to search for an additional significant hotspot (σ_2), if present as shown in Fig.2.

The analysis of intermediate-scale anisotropies in the Pierre Auger Observatory data reveals a prominent hotspot in the Centaurus region with a significance of 5.2σ within a search window of $\Psi_1 = 24°$. The significance of the secondary overdensity is 3.4σ comparable to the value expected for an isotropic sky, suggesting that no other dominant structures remain in the UHECR sky once the primary hotspot is excluded. In this case, the largest deviation from isotropy is maximized by a search window $\Psi_2 = 12°$.

A significant discrepancy arises in some datasets, in particular when using the `JF12` model with a large source fraction: the primary overdensity in the Centaurus region, mostly due to the SBGs

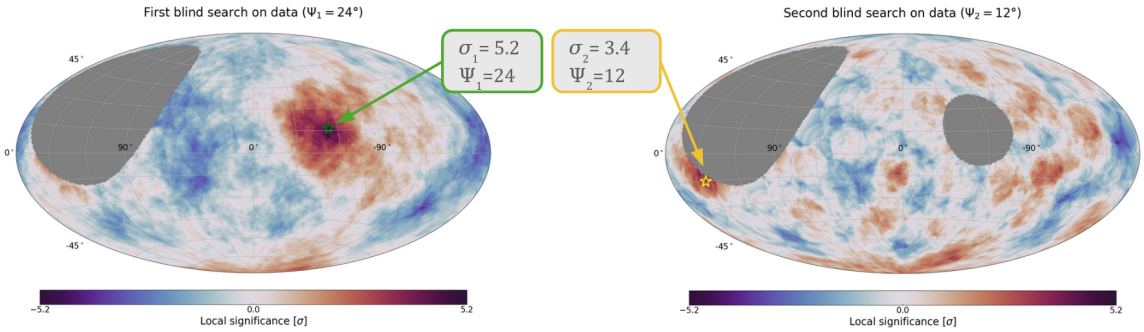

Figure 2: Sequential blind searches applied on data. The green star indicates the position of the highest deviation from the isotropic expectation in the first blind search while the yellow star indicates the largest excess in the second blind search. The search window employed to display the local significance for the sequential blind searches is indicated with Ψ_1 and Ψ_2.

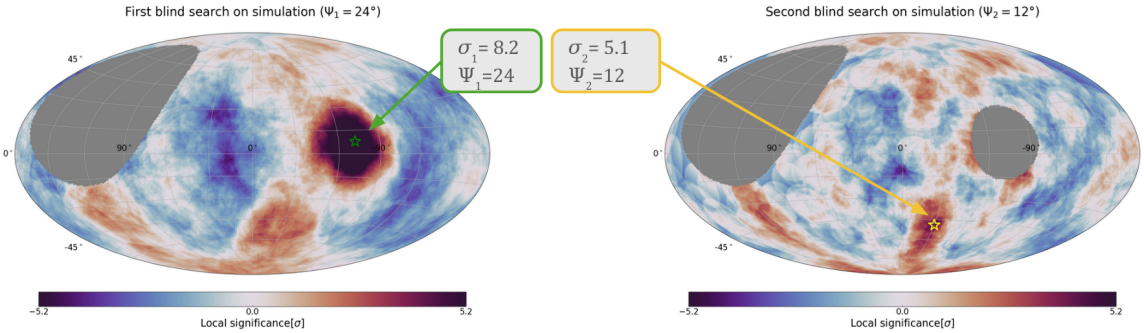

Figure 3: Sequential blind searches applied on simulation with a generated signal fraction of 15%. The green star indicates the position of the highest deviation from the isotropic expectation in the first blind search while the yellow star indicates the largest excess in the second blind search. The search window employed to display the local significance for the sequential blind searches is indicated with Ψ_1 and Ψ_2.

NGC4945 and M83, is largely amplified and misplaced due to a clusterization of events caused by GMF deflections. Depending on the chosen anisotropic fraction, in up to 30% of realizations when employing `JF12` as GMF model, substantial secondary structures, mostly due to NGC253 and NGC1068, persist even after the exclusion of the primary hotspot as presented in Fig. 3. This overestimation of clustering provides useful information to constrain the strength of the EGMF [11, 12]. When introduced, the EGMF is expected to reduce event clustering, and its impact can be quantified by setting observationally motivated limits [13]. Specifically, if a sufficiently strong EGMF suppresses the secondary overdensity to levels consistent with observations, it establishes a lower limit. Conversely, if the EGMF is strong enough to significantly disperse the primary overdensity in the Centaurus region, it defines an upper limit. To account for the EMGF deflections, we apply an angular deflection, following a von Mises-Fisher distribution, at the edge of the Galaxy, modeled as a function of rigidity and source distance:

$$\theta_{ij}^{\mathrm{eg}} = \theta_0 \sqrt{\frac{D_i}{D_0}} \frac{R_0}{R_j}, \tag{3}$$

where D_i is the distance to the source, and R_j is the rigidity of the injected cosmic ray. The

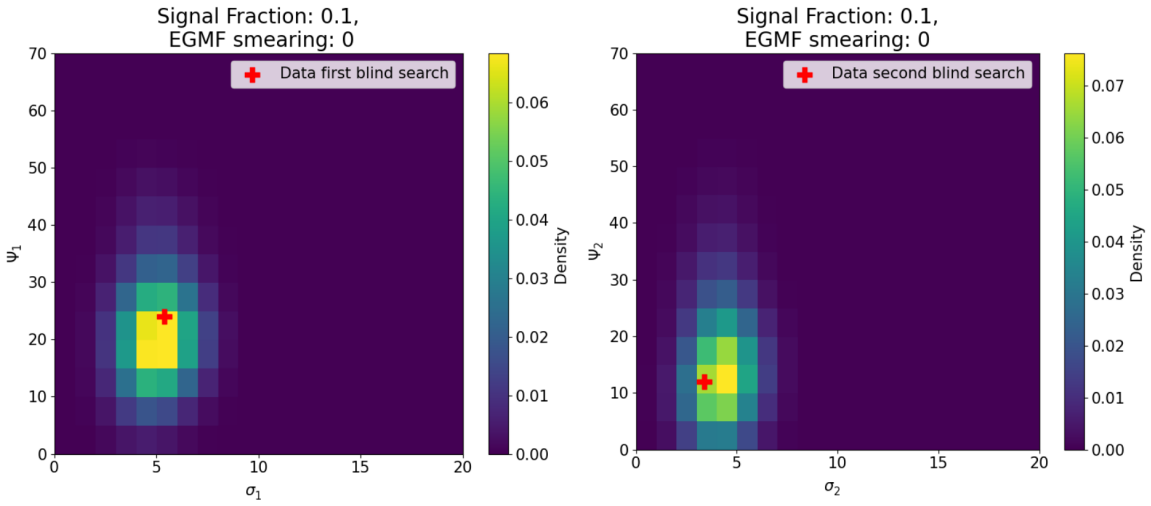

Figure 4: Behavior of the correlated parameters (σ_1, Ψ_1) and (σ_2, Ψ_2) compared to observed data values under the assumption of the `JF12` model for $f_{\rm sgn} = 0.1$ and $\theta_0 = 0$. The red crosses indicate the observed data values, highlighting the points requiring further analysis within the likelihood framework.

reference values are set to $D_0 = 3.47$ Mpc and $R_0 = 40/7$ EV, corresponding to the distance of NGC 4945 and the rigidity of a Nitrogen (Z=7) nucleus at 40 EeV, chosen for normalization near the energy threshold of the analysis. The parameter θ_0 remains free in this study. This model follows the expectations for small-angle scattering in a turbulent EGMF, as discussed in Ref.[14].

By varying θ_0 from 0° to 80°, we analyzed the behavior of the anisotropy parameters (σ_1, Ψ_1) and (σ_2, Ψ_2) by comparing them to the values obtained from data. This comparison is quantified through the deviance, defined as:

$$\sqrt{D - D_{\rm min}} = \sqrt{-2\ln(\mathcal{L}_1) - 2\ln(\mathcal{L}_2) + 2\ln(\mathcal{L}_{\rm min})} \tag{4}$$

where $\ln(\mathcal{L}_1)$ and $\ln(\mathcal{L}_2)$ correspond to the log-probability density values at the positions of the red crosses shown in the left and right panels of Fig. 4, respectively. That is,

$$\ln(\mathcal{L}_i) = \ln P(\sigma_i^{\rm data}, \psi_i^{\rm data}), \tag{5}$$

where P represents the joint probability density from simulations for overdensity i, evaluated at the observed data values.

The results show that with a low source contribution and no EGMF, the first blind search applied to simulations provides good agreement with observations, indicating that the observed anisotropy can be reproduced with minimal EGMF effects. However, the second blind search reveals a small tension: simulations tend to exhibit a second overdensity with a higher average local significance than observed. This suggests that a stronger EGMF contribution could slightly improve the agreement of data and simulation. However, given the current precision of the data, no significant lower limit can be established.

The approach presented in this work can be used to establish constraints on the strength of the EGMF by analyzing the clustering properties of UHECRs. By comparing the observed local significance of overdensities with simulations under different assumptions for the EGMF, we can

identify both lower and upper bounds on its influence. A detailed study expanding on these findings is currently in preparation, where we will further investigate the robustness of our conclusions under different astrophysical scenarios.

4. Conclusion

We have presented an analysis of the arrival directions of UHECRs, incorporating the effects of both Galactic and extragalactic magnetic fields. The maximum likelihood analysis demonstrates that, in a large fraction of simulated datasets, it is possible to recover the results reported by the Pierre Auger Collaboration even when accounting for the influence of the GMF. However, due to the magnetic deflections of heavy elements that dominate the spectrum at high energies, the true contribution from the sources is likely larger than what is inferred from the data.

Furthermore, we have demonstrated the sensitivity of UHECR arrival directions to the properties of the EGMF. Our findings indicate that the level of clustering observed in the data can be influenced by the interplay between source distributions and magnetic deflections. Future studies will extend this work by investigating the impact of GMF uncertainties, including variations in the coherent and turbulent components, to assess their influence on the observed anisotropy patterns [15].

References

[1] C. Lunardini et al. *JCAP*, 10:073, 2019. doi:10.1088/1475-7516/2019/10/073.

[2] P. Abreu et al. [Pierre Auger Collaboration]. *ApJ*, 935(2):170, 2022. doi:10.3847/1538-4357/ac7d4e.

[3] A. Aab et al. [Pierre Auger Collaboration]. *JCAP*, 2017(04):038, 2017. doi:10.1088/1475-7516/2017/04/038 .

[4] R. Batista et al. *JCAP*, 2022(09):035, 2022. doi:10.1088/1475-7516/2022/09/035.

[5] R. Jansson and G. R. Farrar. *ApJ*, 757(1):14, 2012. doi:10.1088/0004-637X/757/1/14.

[6] M. Unger and G. R. Farrar. *ApJ*, 970(1):95, 2024. doi:10.3847/1538-4357/ad4a54.

[7] R. Jansson and G. R. Farrar. *ApJ letter*, 761(1):L11, 2012. doi:10.1088/2041-8205/761/1/l11.

[8] R. Adam et al. [Planck Collaboration]. *A&A*, 596:A103, 2016. doi:10.1051/0004-6361/201528033.

[9] H. Bretz et al. *ApJ*, 54:110, 2014. doi:10.1016/j.astropartphys.2013.12.002.

[10] R. Higuchi et al. *ApJ*, 949(2):107, 2023. doi:10.3847/1538-4357/acc739.

[11] J. D. Bray and A. M. M. Scaife. *ApJ*, 861(1):3, 2018. doi: 10.3847/1538-4357/aac777 .

[12] A. van Vliet et al. *MNRAS*, 510(1):1289, 2022. doi:10.1093/mnras/stab3495.

[13] A. Neronov et al. *PRD*, 108(10):103008, 2023. doi:10.1103/PhysRevD.108.103008.

[14] D. Harari et al. *JHEP*, 03:045, 2002. doi:10.1088/1126-6708/2002/03/045.

[15] L. Deval et al. *In preparation*, 2025.